White-light interferometric microscopy for wafer defect inspection

Renjie Zhou[a,b,c], Chris Edwards[a,b], Casey Bryniarski[a], Marjorie F. Dallmann[a], Gabriel Popescu[b] and Lynford L. Goddard*[a]

[a]Micro and Nanotechnology Laboratory, Department of Electrical and Computer Engineering University of Illinois at Urbana-Champaign, Urbana, Illinois 61801, USA

[b]Quantitative Light Imaging Laboratory, Department of Electrical and Computer Engineering Beckman Institute for Advanced Science and Technology University of Illinois at Urbana-Champaign, Urbana, Illinois 61801, USA

[c]Currently with George R. Harrison Spectroscopy Laboratory, Massachusetts Institute of Technology, Cambridge, Massachusetts 02194, USA

ABSTRACT

White-light imaging systems are free of laser-speckle. Thus, they offer high sensitivity for optical defect metrology, especially when used with interferometry based quantitative phase imaging. This can be a potential solution for wafer inspection beyond the 9 nm node. Recently, we built a white-light epi-illumination diffraction phase microscopy (epi-wDPM) for wafer defect inspection. The system is also equipped with an XYZ scanning stage and real-time processing. Preliminary results have demonstrated detection of 15 nm by 90 nm in a 9 nm node densely patterned wafer with bright-field imaging. Currently, we are implementing phase imaging with epi-wDPM for additional sensitivity.

Keywords: Wafer defect inspection, interferometric microscopy, quantitative phase imaging, white-light defect inspection, image post-processing

1. INTRODUCTION

Laser quantitative phase imaging (QPI), a sensitive imaging technique, has been widely used in the past for biological and material science imaging [1-3]. In recent years, we have also applied QPI for patterned wafer defect inspection, looking at patterning defects that are smaller than 20 nm wide by 100 nm long [4-6]. However, the laser-speckle has hindered laser QPI for detecting defects that are smaller than 10 nm wide. Over the past year, we have developed a white-light QPI technique to address the future needs in defect inspection metrology. This system is based on the principle of white-light diffraction phase microscopy [7-9]. Our system has a spatial coherence area of about the diffraction spot, which is sufficient for inspecting densely patterned wafers. In addition to phase imaging, we also added automated XYZ scanning of the wafer, enabling pixel level wafer translation during the imaging. In-plane and vertical through focus wafer scans are made possible with a LabVIEW interface that also integrates the image retrieval processing and thus enables real-time defect inspection.

2. WHITE-LIGHT INSPECTION SYSTEM

Before building the white-light interferometry inspection system, we first build a white-light bright-field inspection system. This system is equipped with XYZ scanning, and our results showed that we can clearly detect 15 nm by 90 nm defects in a 9 nm node densely patterned wafer. In order to perform white-light interferometry, or epi-wDPM in particular, we need a white-light source and a Fourier plane filter to make the reference beam and the signal beam. The white-light source we decided to use is a cold white-light LED (Thorlabs MCWHL5 source, cold means the spectrum is close to blue) with 800 mW maximum output power. The spectrum of this light source is plotted in Fig. 1 (data from Thorlabs). The spectrum has an abnormal and non-symmetric profile. When measuring the sample surface profile, we need to know the mean wavelength of the light source. Using the spectrum data, we determined the source has a mean wavelength at 503 nm. It is also necessary to measure the temporal coherence length, which limits the maximum surface height measurement and also relates to speckle effect. For such a non-symmetric spectrum, we use the power equivalent spectrum bandwidth $\Delta\lambda = |\lambda_{max}-\lambda_{min}|$ to calculate the temporal coherence length $l_c = \lambda_{max}\,\lambda_{min}/\,\Delta\lambda$. The λ_{max} and λ_{min} values are calculated to be 532.2 nm and 473.2 nm, thus l_c is found to be ~ 4.3 μm.

*lgoddard@illinois.edu; phone 1 217 244-0799; fax 1 217 244-6375; http://psl.mntl.illinois.edu

Quantitative Phase Imaging, edited by Gabriel Popescu, YongKeun Park, Proc. of SPIE Vol. 9336, 93362P · © 2015 SPIE · CCC code: 1605-7422/15/$18 · doi: 10.1117/12.2079660

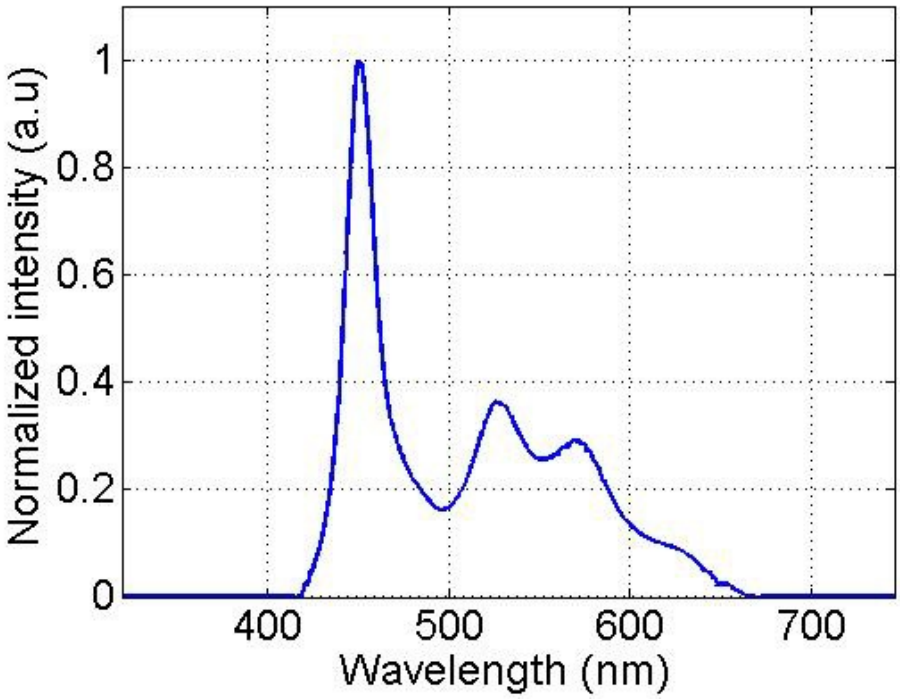

Figure 1. The Thorlabs cold white-light LED spectrum.

For the Fourier plane filter, we follow the previously demonstrated white-light DPM (wDPM) design [7-9]. The Fourier space filtering is performed with a projector-based spatial-light modulator (SLM). In white-light phase imaging, the spatial coherence is an important factor to consider. Through proper spatial filtering, one needs to achieve a spatial coherence area larger than the field of view to get the correct quantitative phase imaging results. It was found that both the aperture diaphragm (relates to the illumination beam) and the SLM filtering are equally important for achieving the proper spatial coherence, as described in references [8, 10]. According to these references [8, 10], the measured phase is the true phase subtracting the low-pass filtered phase due to the filter and illumination, which can be expressed as

$$\phi(\mathbf{r}) = \arg\left[S(\mathbf{r})\right] - \arg\left\{\left[T_{ill}^{*}(\mathbf{r})\tilde{T}_{ref}(\mathbf{r})\right] \otimes S(\mathbf{r})\right\}, \tag{1}$$

where S is the sample reflection function, T_{ref} is the SLM reference pinhole aperture function (tilde denotes Fourier transform), and T_{ill} is the illumination mutual intensity function. By assuming a shift-invariant illumination field, we can defined T_{ill} as

$$T_{ill}\left(\mathbf{r}-\mathbf{r}'\right) = \left\langle U_{ill}(\mathbf{r},t)U_{ill}^{*}\left(\mathbf{r}',t\right)\right\rangle_{\tau}, \tag{2}$$

where U_{ill} is the sample illumination field selected by the aperture diaphragm T_{ap}, as

$$U_{ill}(\mathbf{r},t) = \tilde{U}_{s}(\mathbf{r},t) \otimes \tilde{T}_{ap}(\mathbf{r}). \tag{3}$$

Note that T_{ill} and T_{ref} are not independent of each other, a smaller aperture diaphragm makes it easier to make a smaller reference beam filter, this is reflected by the product $T_{ill}^{*}(\mathbf{r})\tilde{T}_{ref}(\mathbf{r})$ in Eq. (1). In Eq. (1), the first term $\arg\left[S(\mathbf{r})\right]$ is the true phase of the sample. Notice that the true phase may not be the surface profile of the object, depending on the internal object structure. The second term $\arg\left\{\left[T_{ill}^{*}(\mathbf{r})\tilde{T}_{ref}(\mathbf{r})\right] \otimes S(\mathbf{r})\right\}$ is the low-pass filtered version of the true phase. Thus, the overall phase is high-pass filtered. Ideally, we need both $T_{ill}(\mathbf{r})$ and $T_{ref}(\mathbf{r})$ to be uniform (both the aperture diaphragm

and the SLM pinhole filter to be delta functions), then the second term becomes a constant that can be removed through calibration. However, this is impractical, because almost all the power of the light source will be blocked, resulting in a noisy interference image. In reality, the aperture diaphragm will have a certain size that compromises the coherence and power, and the SLM pinhole filter will have a certain size to balance the fringe contrast and power. To determine the coherence area of the system, we need to measure the numerical aperture (NA) of the aperture diaphragm, which can be done in its conjugate plane on the SLM. On the sample stage, we can use a diffusive objective to fill the resolution circle in the signal beam in the 1st-diffraction order. The white-light source selected by the aperture diaphragm will also show up in this diffraction order. Thus, by measuring the ratio σ, defined as the resolution circle diameter over the light source circle diameter, the spatial coherence length can be determined as d_{airy}/σ, where d_{airy} is the Airy spot (or diffraction spot) diameter, $d_{\text{airy}} = 1.22\lambda_{mean}/NA_{\text{obj}}$. For a fully coherent source σ is 0, thus infinite coherence, whereas for a completely incoherent source σ equals to 1 that corresponds to a coherence length of the diffraction spot. Thus, in white-light bright-field imaging, with no light source filtering, the objective lens determines the coherence length.

In most cases, having a spatial coherence area to cover the field of view is difficult to obtain [8]. Practically, we can just achieve full spatial coherence over the sample area. For cell imaging, a spatial coherence length of ~ 10 μm is usually sufficient, while for patterned wafer defect inspection a coherence length of a diffraction spot is sufficient since the features are typically sub-wavelength. Thus, for the wafer inspection experiments, the coherence is not an issue for phase imaging. However, it is still desirable to have relatively good image contrast through reducing the aperture diaphragm NA at the expense of light power.

In our system, to trade beam power for contrast, the aperture diaphragm is closed down to ~ 1 mm (the minimum) to select the light source, which is crucial for spatial coherence. For wafer inspection, the wafer structures are usually smaller than the diffraction spot, thus, the spatial coherence is not a big issue. However, closing down the aperture diaphragm is still necessary to obtain the optimum image contrast. On the SLM plane, we gradually shrunk the size of the reference beam pinhole filter to get a plane wave, at least across the camera sensor area, for making a reference beam. However, as the pinhole size gets smaller, the reference beam power decreases significantly, resulting in poor fringe visibility on the camera. To maintain relatively good visibility, we have to use a pinhole of about 200 μm. However, this induces a high-pass filtering effect in the phase image as we discussed earlier. This high-pass filtering effect is notorious for large sample structures, but can actually be helpful in defect inspection where structures are tiny and defects are sharp. The high-pass filtering provides edge detection in the optical domain.

3. REAL-TIME INSPECTION SYSTEM

For wafer defect inspection, a precise and automated XYZ 3D sample scanning stage is necessary. It is also desirable to have a real-time inspection system that can integrate the camera image acquisition, XYZ sample stage control, and image post-processing into a single graphic user interface (GUI). Over the past year, we have been able to implement such a system in NI LabVIEW as illustrated in Fig. 2. The XYZ stage is assembled from three separate actuator-based translation stages (Thorlabs, ZST225B) with 25 mm travel distance and 8 nm minimum step size. In addition to the XYZ stages, we also have tip, tilt, and rotation correction. The XYZ stage is fitted onto the Zeiss Axiovert inverted microscope with a custom machined stage. This system is capable of performing wafer scans with specified step size, direction, and range. It can also perform sequential scans in different directions.

In the real-time processing LabVIEW program, the camera control uses the NI Vision module and the Hamamatsu video capture library. The XYZ stage motors are controlled with the Thorlabs software through LabVIEW. The image processing is done mostly with the NI CUDA module (such as performing Fourier transforms) with the most efficient image retrieval algorithm. CUDA is designed for parallel computation in a GPU by NVIDIA. In order to use the NI CUDA module, an NVIDIA certified GPU is installed. The image post-processing takes about 210 ms which includes retrieving the phase and amplitude image and computing the histogram and the fringe visibility curve. The camera (Hamamatsu C4742-80-12AG) image acquisition takes about 125 ms. Thus, the overall time for one image capture takes about 500 ms for small scanning steps which corresponds to 2 frame/s. The real-time processing program can also be used for system alignment in DPM. In fact, we have also been able to integrate an automatic pinhole alignment program to a DPM system to make the system more user friendly.

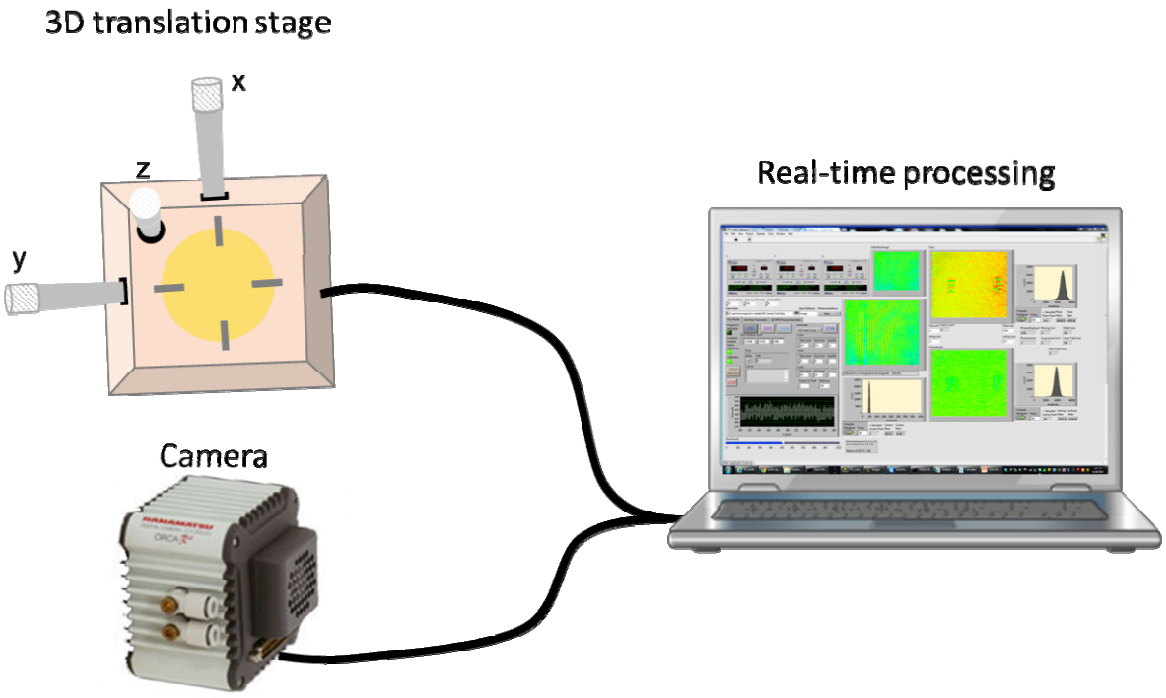

Figure 2. Illustration of the real-time defect inspection system.

4. WHITE-LIGHT INTERFEROMETRIC SYSTEM TEST

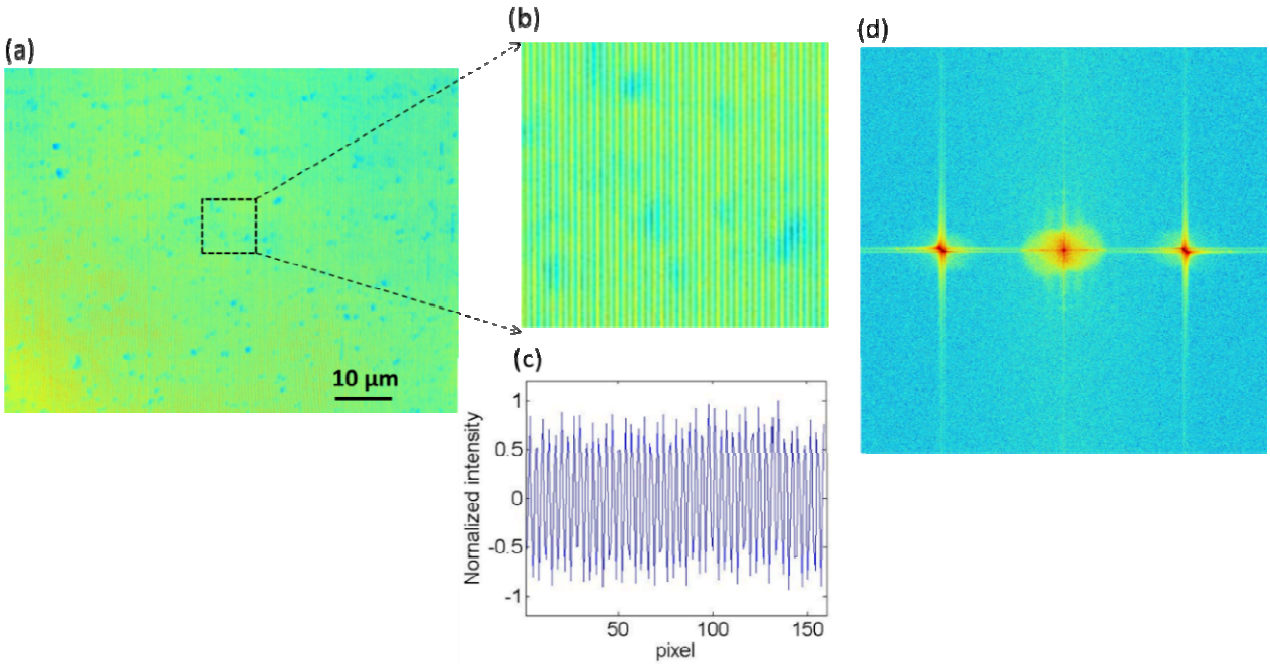

Figure 3. Fringe contrast analysis of the epi-wDPM system. (a) An interferogram on a flat sample region. (b) A zoomed-in potion of the interferogram. (c) The intensity along the horizontal dimension with the vertical dimension averaged. (c) The Fourier spectrum of the interferogram.

In this section, we show the white-light inspection system testing results using the real-time white-light QPI system we have built. Before imaging test samples, we first check the fringe contrast and the Fourier spectrum of the fringes, as shown in Fig. 3. Figure 3(a) is an interferogram taken on a flat sample, Fig. 3(b) is a zoomed-in portion of the interferogram, Fig. 3(c) is a normalized fringe profile plot along the horizontal dimension of the zoomed-in interferogram with averaging in the vertical dimension, and Fig. 3(d) is the log-scale plot of the interferogram Fourier spectrum magnitude, where we see three beam orders are clearly separated as expected. From the analysis, we conclude that good fringe contrast has been achieved.

With good fringe contrast, we started to perform tests on a photo-lithography defined silicon sample which has different structures with about 25 nm designed height. In Fig. 4, we measure a horizontal alignment sample in amplitude and phase in Fig. 4 (a) and (b), and a vertical alignment sample in Fig. 4(c) and (d), where 2 μm wide lines are gradually dislodged starting from the center. The full structures start to show up, indicting almost sufficient spatial coherence. The measured heights of the structures from the surface profile images are close to the designed 25 nm, but not exactly correct. Several reasons may account for this, such as misalignment and lack of spatial coherence in the system. It is also possible that the samples were not fabricated perfectly. To validate the epi-wDPM measurement data, SEM and alpha-step measurements are needed. In the future, we plan to use this system for 9 nm node wafer defect inspection.

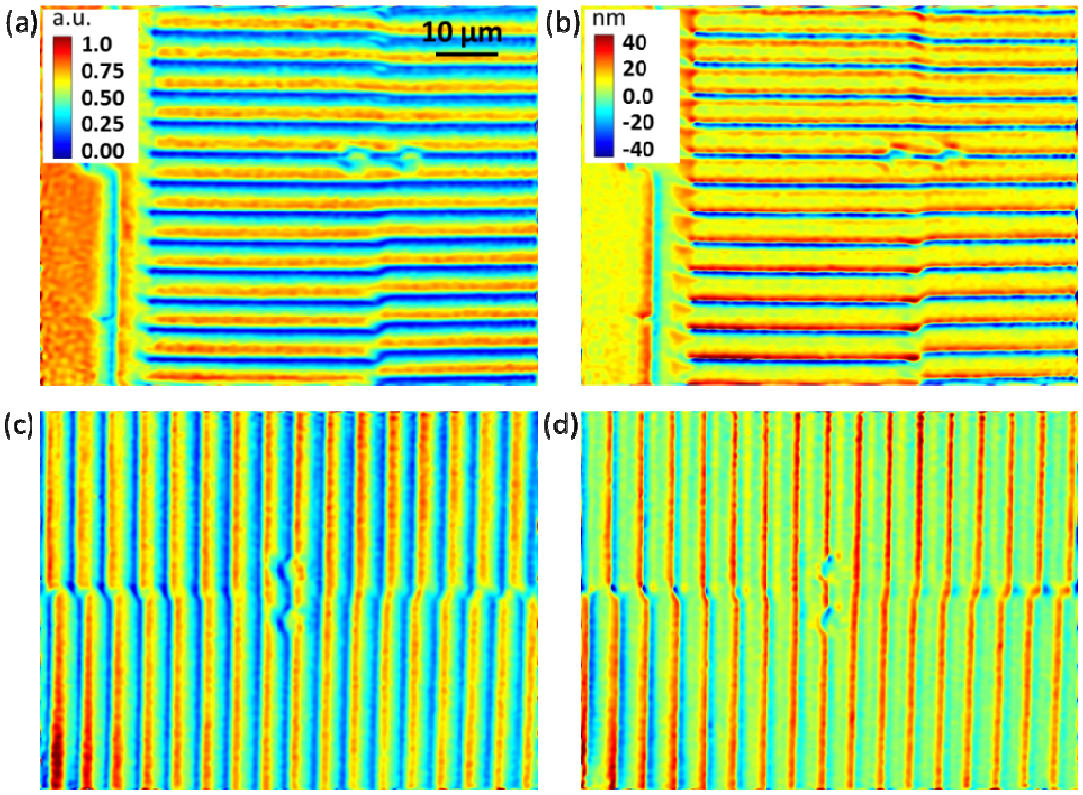

Figure 4. Test measurement of two alignment structures. (a) Amplitude image of the horizontal alignment sample. (b) Surface profile of the horizontal alignment sample. (c) Amplitude image of the vertical alignment sample. (d) Surface profile of the vertical alignment sample.

5. CONCLUSION

We have built a white-light interferometry system for wafer defect inspection. The working principles are briefly discussed. For this system, a user GUI is also designed for real-time defect inspection. Using this real-time system, we demonstrated phase imaging of 25 nm high silicon photo-lithography structures with 2 μm feature size. In the future, we plan to implement our system for 9 nm node wafer defect inspection.

ACKNOWLEDGMENTS

We would like to acknowledge the major support from Semiconductor Research Corporation (contract P13117) and National Science Foundation (grant CBET-1040462 MRI) with matching funds from the University of Illinois. In addition, RZ was supported by a Beckman graduate fellowship by the Arnold and Mabel Beckman Foundation.

REFERENCES

[1] Bhaduri, B., Edwards, C., Pham, H., Zhou, R., Nguyen, T. H., Goddard, L. L. and Popescu, G., "Diffraction phase microscopy: principles and applications in materials and life sciences," Adv Opt Photonics **6**, 57-119 (2014).

[2] Edwards, C., Arbabi, A., Popescu, G. and Goddard, L. L., "Optically monitoring and controlling nanoscale topography during semiconductor etching," Light Sci Appl **1**, e30 (2012).

[3] Kim, T., Zhou, R., Goddard, L. L. and Popescu, G., "Breakthroughs in Photonics 2013: Quantitative Phase Imaging: Metrology Meets Biology," IEEE Photonics Journal **6**, 1-9 (2014).

[4] Zhou, R., Popescu, G. and Goddard, L. L., "22 nm node wafer inspection using diffraction phase microscopy and image post-processing," SPIE **8681**, 86810G (2013).

[5] Zhou, R., Edwards, C., Arbabi, A., Popescu, G. and Goddard, L. L., "Detecting 20 nm wide defects in large area nanopatterns using optical interferometric microscopy," Nano Lett **13**, 3716-3721 (2013).

[6] Zhou, R., Edwards, C., Popescu, G. and Goddard, L. L., "9nm node wafer defect inspection using visible light," Proc. SPIE **9050**, 905017 (2014).

[7] Bhaduri, B., Pham, H., Mir, M. and Popescu, G., "Diffraction phase microscopy with white light," Opt Lett **37**, 1094-1096 (2012).

[8] Edwards, C., Bhaduri, B., Nguyen, T., Griffin, B., Pham, H., Kim, T., Popescu, G. and Goddard, L. L., "The effects of spatial coherence in diffraction phase microscopy," Opt. Exp. **22**, 5133-5146 (2014).

[9] Edwards, C., Bhaduri, B., Griffin, B. G., Goddard, L. L. and Popescu, G., "Epi-illumination diffraction phase microscopy with white light," Opt Lett **39**, 6162-6165 (2014).

[10] Nguyen, T., Edwards, C., Goddard, L. L. and Popescu, G., "Quantitative phase imaging with partially coherent illumination," Opt Lett **39**, 5511-5514 (2014).